Photoluminescence and Photoconductivity of ZnS-Coated ZnO Nanowires

Ashok Bera and Durga Basak*

Department of Solid State Physics, Indian Association for the Cultivation of Science, Jadavpur, Kolkata 700032, India

ABSTRACT ZnO nanowires (NWs) with a ZnS coating are synthesized in order to modify the surface without changing the diameter of the NWs. They have the wurtzite ZnO at the core and a cubic ZnS at the outer layer. The NWs show a sharp ultraviolet and a broad visible emission of the photoluminescence spectra. Surface modification has led to a change in the position of the maxima of the visible emission in ZnO−ZnS NWs. The photocarrier relaxation under steady UV illumination occurs in ZnO NW arrays but is absent in ZnO−ZnS NW arrays. The dark current value for both type of NWs are similar, whereas the photocurrent value is much higher in the surface-modified NWs. Higher photocurrent value indicates a transport of the photogenerated carriers from the ZnS layer to ZnO during UV illumination. The carrier transport mechanism is proposed through a model.

KEYWORDS: surface modification • nanowires • optoelectronic properties • ultraviolet • ZnO−ZnS;

INTRODUCTION

Zinc oxide (ZnO), a unique material for its wide band gap (3.3 eV) and piezoelectric properties, has been widely investigated for applications in UV detectors (1, 2) and light emitters (3), transparent conductive films (4), and piezoelectric nanogenerator (5). Recently, one-dimensional and quasi-one-dimensional (Q1D) ZnO nanostructures have attracted a great deal of attention because of their unique nanoscale electronic and optoelectronic properties as well as technological applications (6−8). The electrical, optical, and magnetic properties of ZnO can be adjusted desirably not only by impurity doping but also through surface modification (9−14). The modification of the surface is considered as one of the advanced techniques to change the physical properties of ZnO for a better nanoscale application (13−18). In previous reports, we have shown that the aqueous chemically grown Q1D ZnO NWs show decay in the photocurrent through a two-electron process under steady UV illumination and discussed the role of the surface states in such carrier relaxation (19, 20). When the surfaces of these NWs are capped with poly vinyl alcohol (PVA), the extent of carrier relaxation is decreased and the total photocurrent gain, i.e., photo (I_{ph})-to-dark current (I_D) ratio, is increased (21). There are few reports on ZnO coated with ZnS or ZnS coated with ZnO (22−25). Li et al. (22) have shown better emission properties when ZnO NWs are coated with ZnS (ZnO−ZnS NWs). The conversion of electrical energy from mechanical energy using ZnO−ZnS NWs demonstrates excellent application of surface-modified nanoscale materials (23). Wang et al. (25) have detailed on the microstructure of synthesized epitaxially grown ZnO NWs on ZnS by vapor phase transport. However, study on the

electro-optic properties of ZnO−ZnS is not available in the literature. Therefore, in this paper, we study mainly the photoluminescence and photoconduting properties of ZnO−ZnS NWs. We show that when surfaces of ZnO NWs' are converted to ZnS, the decay in the photocurrent during steady UV illumination is totally absent and a very high photocurrent value has been achieved that indicates that ZnO−ZnS NWs show improved UV photosensitivity.

EXPERIMENTAL SECTION

The quasi-vertical ZnO NWs were grown on the glass substrates following the ACG method as described elsewhere (19). In brief, we first deposited a ZnO seed layer by coating with a solution of zinc acetate and thermally decomposing it at 350 °C. Then the NWs were grown by dipping the substrates with the seed layer in an equimolar mixture of $(CH_3COO)_2Zn \cdot 2H_2O$ and hexamethylenetetramine $(CH_2)_6N_4$ (20 mM) in deionized water at 90 °C for 1 h. The substrates were then removed from the solution, rinsed in deionized water and dried. For ZnS capping, the previously prepared ZnO NWs were dipped into 50 mL of 10 mM aqueous solution of thioacetamide (TAA) (Sigma-Aldrich) at 70 °C for 1 h and then dried. For increasing the ZnS capping, the ZnO NWs are dipped in the TAA solution at same temperature for about 2 h. The crystalline phase and the morphology were confirmed by X-ray diffractometer (model Bruker D8), field-emission scanning electron microscopy (FESEM, model JEOL JSM-6700F), and high-resolution transmission electron microscopy (HRTEM, model JEM 2010). The optical excitation of the samples during the photoluminescence (PL) measurements was done by a monochromatic light of wavelength 325 nm from a He−Cd laser (Kimmon Koha Co., Ltd.; model KR1801C) with a 90 mW power irradiance on the sample. A high-resolution spectrometer (Horiba Jobin Yvon, Model: iHR 320) together with a photomultiplier tube was used to detect the luminescence from the samples. For the photoresponse measurements, two gold electrodes (of 50 nm thickness) were thermally evaporated in circular form with a diameter of 1 mm through a shadow mask at a separation of 3 mm on the top of ZnO NWs arrays. The photocurrent was measured by illuminating the NWs with a monochromatic light from a xenon lamp operating at 150 W using a spectral illuminator system (model 69050, New-port Corp, USA) under 3 V bias conditions.
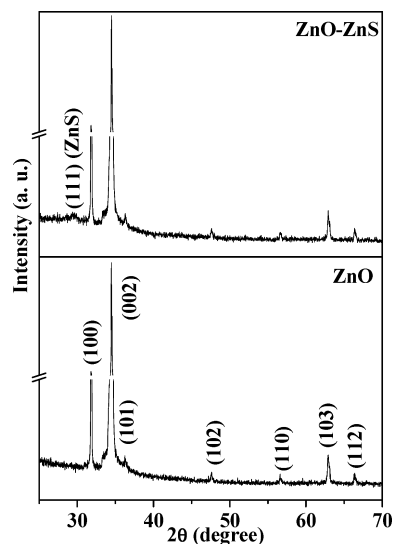
FIGURE 1. XRD patterns of ZnO and ZnO−ZnS NWs.

The current was measured using the Keithley source meter (model 2400).

RESULT AND DISCUSSION

The X-ray diffractogram of ZnO and ZnO−ZnS NWs arrays in Figure 1 shows the presence of hexagonal wurtzite phase of ZnO. Stronger intensity of the (002) peak compared to (100) peak for both the samples indicates that the NWs are nearly aligned along the normal to the substrate. X-ray diffraction pattern of ZnO-ZnS NWs show a small peak at ~$2\theta = 29°$, which corresponds to the (111) peak of cubic ZnS structure. The FESEM images of the NWs arrays (with a substrate inclination by 15°) are shown in Figure 2a,b. The images show almost vertical growth of the NWs, which support the XRD results. A clear difference in the surface morphology of ZnO and ZnO−ZnS NWs can be visualized from the images as the sidewalls of the former are smooth and well-defined, whereas those of the latter are rough and wrinkled indicating some modification has been occurred on the surface. TEM images c and e in Figure 2 show, respectively, the smooth and wrinkled sidewalls for ZnO and ZnO−ZnS NWs, which is similar to the FESEM results. There is no significant change in the diameter of the NWs indicating that only the surface ZnO layer is converted to ZnS. The HRTEM images in Figure 2d,f show the interplanar spacing corresponding to the (100) plane for the wurtzite ZnO and (111) plane of cubic ZnS structure confirming formation of ZnS. Insets in Figure 2c,e show the corresponding selected-area electron diffraction (SAED) patterns of ZnO and ZnO−ZnS NWs, respectively. The SAED pattern of ZnO−ZnS NWs has two sets of spots, weak spots and bright spots, corresponding to the cubic ZnS and wurtzite ZnO structures, respectively. The EDS spectra in Figure 3 show the presence of Zn and O atoms in case of ZnO, whereas additional S atoms are detected in ZnO−ZnS NWs. Therefore, the microstructural composition analyses also indicate that the surfaces of the NWs have been modified to ZnS.

The room temperature photoluminescence spectra of the ZnO and ZnO-ZnS NWs show a very strong UV peak at
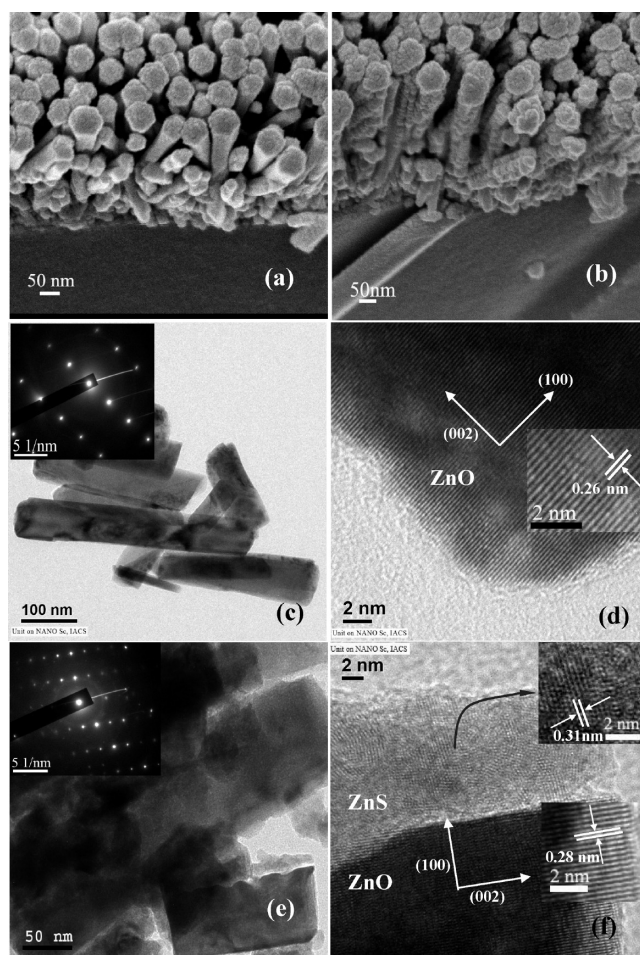

FIGURE 2. (a, b) FESEM images of ZnO and ZnO−ZnS, respectively. (c, d) TEM and HRTEM images of ZnO. (e, f) TEM and HRTEM images of ZnO−ZnS. The insets of c and e give the SEAD patterns of ZnO and ZnO−ZnS, respectively.

around 375 nm and a broad visible emission in the region 500 to 700 nm (Figure 4). The UV peak position of the ZnO−ZnS structures show a slight red shift compared to ZnO NWs, which is similar to the results of Zhu et al. (23). Gaussian multipeak fitting of the broad visible emissions in the photoluminescence spectra of both ZnO and the ZnO-ZnS NWs shows the presence of a higher intense peak at ~600 nm, which is attributed to the presence of excess oxygen/water molecules on the surface of ZnO NWs (26, 27), while a peak at ~500 nm becomes prominent in case of ZnO−ZnS NWs (see the Supporting Information, Figure S1). The 500 nm peak in the latter may be due to the defect emissions of ZnO and ZnS. The above results indicate that after the formation of a ZnS layer on the surface, the nature of visible emission is changed.

The schematic arrangement for the photocurrent measurements is shown in the Supporting Information, Figure S2. Photocurrent growth and decay were measured in the air ambient by switching the UV illumination (370 nm) "on" and "off" for 15 min each (Figure 5). On UV illumination, the photocurrent in ZnO NWs reaches a maximum value of 3.18×10^{-5} A within a few seconds and then it starts decaying during steady UV illumination. The photocurrent decreases by almost 50 % of its maximum value during 15
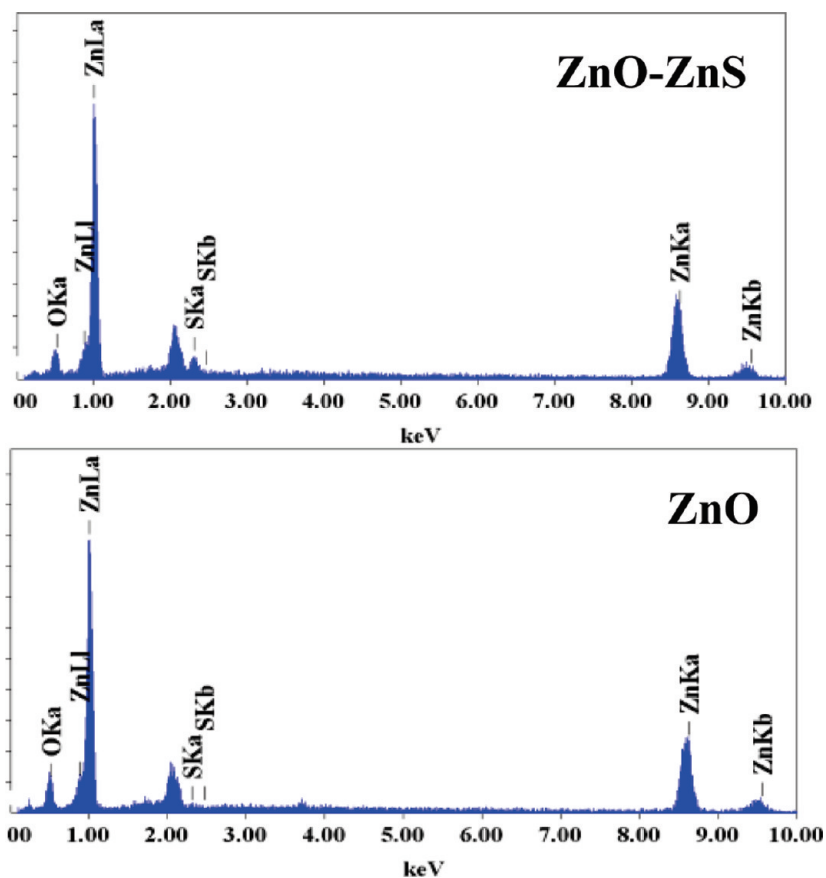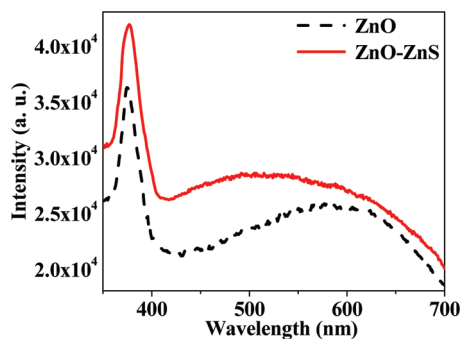
FIGURE 3. EDS spectrum of ZnO and ZnO–ZnS NWs.

FIGURE 4. Photoluminescence spectra of ZnO and ZnO–ZnS NWs.

FIGURE 5. Semi log plot of the photocurrent transient spectra of ZnO and ZnO–ZnS NWs on illumination of the monochromatic light of wavelength 370 nm. The inset shows the growth and decay in linear scale and corresponding biexponential fitting (solid red line) for the decay part for the ZnO NWs.

min of the steady illumination and reaches a value of 1.58×10^{-5} A. It is known that the surface-adsorbed O_2 and water molecules largely affect the photoresponse of the NWs when the surface-to-volume ratio is high (28). O_2 molecules chemisorbed and physisorbed on the NWs surfaces get ionized as O_2^- by trapping electrons from the NWs that result in the formation of a depletion layer causing a band bending toward upward. This leads to a barrier height for the electrical conduction. On illumination, the photoexcited holes are generated and are trapped by the adsorbed O_2^- through the surface electron–hole recombination, although the photoexcited unpaired electrons significantly increase the conductivity due to the increased lifetime (1). The photocurrent decay under steady illumination occurs through a two-electron process. One is electron capture by the surface states and the other is electron recombination at the deep
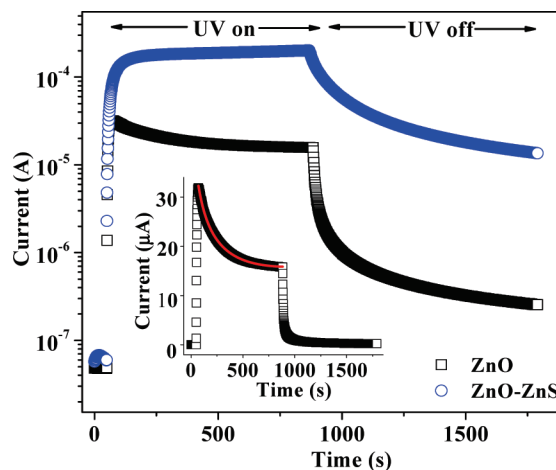
defect states Zn_i^{+2}, which is present because of otherwise formed V_{Zn}–H_2O complex on the surface in the presence of adsorbed H_2O molecules instead of forming a Zn_i^{+2}–V_{Zn}^{-2} defect. Detailed discussion on the reason of photocurrent decay during steady UV illumination had been presented in the previous report (20). Therefore, the decay in the photocurrent can be well-fitted with a biexponential decay equation (inset of Figure 5) of the type given below as reported earlier (19, 20)

$$I = I_0 + Ae^{-t/\tau_1} + Be^{-t/\tau_2} \qquad (1)$$

where τ_1 (42 s) and τ_2 (200 s) are the faster and slower decay time constants, respectively. But, interestingly, there is no such photocurrent decay in ZnO−ZnS NWs, which rather shows a much higher photocurrent value of 2.02×10^{-4} A, as shown in the inset of Figure 5. It has been observed that the time taken for the 90% growth and decay of the maximum current are about 10 and 62 s, respectively, for ZnO NWs, whereas the values are 229 and 547 s, respectively, for the ZnO−ZnS NWs. The slower growth and decay in the latter is due to the surface modification. It is well-known that the adsorption and desorption of O_2 molecules makes the photoresponse faster (29). Therefore the slower photoresponse of ZnO−ZnS NWs confirms reduced adsorption and desorption of the O_2 molecules on the modified surfaces because of the presence of a ZnS layer. At the same time, there is a less chance of formation of $V_{Zn}-H_2O$, as the surface of the NW is capped with ZnS, so V_{Zn}^{-2} is free to form $Zn_i^{+2}-V_{Zn}^{-2}$. Though the V_{Zn} may be present in the ZnS layer too, its presence only on the surface may form $V_{Zn}-H_2O$ complexes. However, because of the thinner layer of ZnS, the chances are less. Therefore, because of less $V_{Zn}-H_2O$ formation, the photogenerated electrons are not allowed to recombine at Zn_i^{+2}. As a result, the carrier relaxation during steady UV illumination is diminished. The dark current values are nearly equal for both types of NWs (4.9×10^{-8} A for ZnO and 6.0×10^{-8} A for ZnO-ZnS), whereas the higher photocurrent magnitude for ZnO−ZnS NWs may be due to either surface modification or transport of extra carriers from the ZnS layer to ZnO or both. The photogenerated carriers can easily be transferred from ZnS to ZnO as the electron affinity of ZnO is 4.5 and that of ZnS is 3.9 eV (24). To confirm the photocarrier transport, we have carried out the following experiments.

The photocurrent spectra (Figure 6a) were measured by illuminating the samples with light of different wavelengths from 800 to 300 nm for 1 min each. All the samples show a strong peak at the UV region at 370 nm. The ZnO NWs show a very sharp peak at 370 nm and a peak near 750 nm. The maximum in the photocurrent at 370 nm is due to an increase in the photocarriers because of the band edge absorption and the maximum at 750 nm is due to the release of the carriers from the adsorbed O_2 molecules related trap states on the surface of the ZnO NWs (20). The photocurrent spectrum of ZnO−ZnS shows an extra peak at 310 nm which is due to the band-to-band absorption of ZnS. Therefore, next we have measured the photocurrent transients by illuminating both the samples by the light of wavelength 310 nm (4 eV), which has the energy higher than the band gap energy of both ZnO and ZnS (Figure 6b). In this case, the ZnO−ZnS NWs show a very high photocurrent (1.62×10^{-4} A) compared to ZnO (5.13×10^{-6} A). The photo current gain for ZnO−ZnS is 17 times higher than only ZnO, which is clear from the semilogarithmic plot in Figure 6b. This means that when the UV light with energy more than the band gap values of both ZnO and ZnS is shined, additional
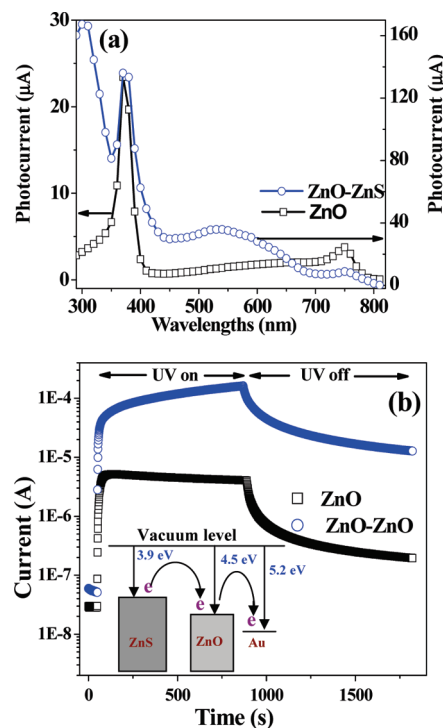

FIGURE 6. (a) Photocurrent spectra at 3 V for ZnO and ZnO−ZnS NWs. (b) Semi log plot of the photocurrent transient spectra of ZnO and ZnO-ZnS NWs on illumination of 310 nm monochromatic light. Inset of the figure gives the electron transport mechanism from ZnS to ZnO.

photocarriers are generated and transferred from ZnS to ZnO, which increases the photocurrent value to a large extent. In fact, it has been observed that the photocurrent value reaches a value as high as several milliamps within 15 min when the S incorporation increases (shown in the Supporting Information, Figure S3). As the S concentration increases, more photocarriers are generated in ZnS, which are transferred from ZnS to ZnO, leading to such a high photocurrent. The carrier transport mechanism is shown in the inset of Figure 6b. As the electron affinity of ZnO is higher than ZnS, the photogenerated electrons are transferred from ZnS to ZnO and then moved to the gold electrodes (electron affinity of 5.2 eV).

CONCLUSION

In summary, we report that ZnO NWs' surfaces can be modified to ZnS, which shows a difference in the position of the visible emission maximum in the PL spectrum. The photocarrier relaxation under steady UV illumination, which occurs in only ZnO NWs, is absent in ZnO−ZnS NWs. The dark current value is similar, whereas the photocurrent value is much higher in the latter. These results indicate that through surface modification by ZnS, the UV photosensitivity can be enhanced in ZnO NWs, which is promising for optoelectronic applications.

REFERENCES AND NOTES

(1) Soci, C.; Zhang, A.; Xiang, B.; Dayeh, S. A.; Aplin, D. P. R.; Park, J.; Bao, X. Y.; Lo, Y. H.; Wang, D. *Nano Lett.* **2007**, *7*, 1003.

(2) Jin, Y.; Wang, J.; Sun, B.; Blakesley, J. C.; Greenham, N. C. *Nano Lett.* **2008**, *8*, 1649.

(3) Sun, X.; Ling, W. B.; Zhao, J. L.; Tan, S. T.; Yang, Y.; Shen, Y. Q.; Dong, Z. L.; Li, X. C. *Appl. Phys. Lett.* **2009**, *95*, 133124.

(4) Cheng, H. C.; Chen, C. F.; Tsay, C. Y. *Appl. Phys. Lett.* **2007**, *90*, 012113.

(5) Xu, S.; Wei, Y.; Liu, J.; Yang, R.; Wang, Z. L. *Nano Lett.* **2008**, *8*, 4027.

(6) Bae, S. Y.; Seo, H. W.; Park, J. *J. Phys. Chem. B* **2004**, *108*, 5206.

(7) Wang, Z. L. *Mater. Today* **2004**, *7*, 26.

(8) Ding, Y.; Wang, Z. L. *J. Phys. Chem. B* **2004**, *108*, 12280.

(9) Zhou, M.; Zhu, H.; Jiao, Y.; Rao, Y.; Hark, S.; Liu, Y.; Peng, L.; Li, Q. *J. Phys. Chem. C* **2009**, *113*, 8945.

(10) Xu, Q.; Schmidt, H.; Zhou, S.; Potzger, K.; Helm, M.; Hochmuth, H.; Lorenz, M.; Setzer, A.; Esquinazi, P.; Meinecke, C.; Grundmann, M. *Appl. Phys. Lett.* **2008**, *92*, 082508.

(11) Jayakumar, O. D.; Sudakar, C.; Persson, C.; Sudarsan, V.; Sakuntala, T.; Naik, R.; Tyagi, A. K. *Cryst. Growth Des.* **2009**, *9*, 4450.

(12) Pereira, A. S.; Ankiewicza, A. O.; Gehlhoff, W.; Hoffmann, A.; Pereira, S.; Trindade, T.; Grundmann, M.; Carmo, M. C.; Sobolev, N. A *J. Appl. Phys.* **2008**, *103*, 07D140.

(13) Shi, L.; Xu, Y.; Hark, S.; Liu, Y.; Wang, S.; Peng, L.; Wong, K.; Li, Q. *Nano Lett.* **2007**, *7*, 3559.

(14) Ra, H. W.; Khan, R.; Kim, J. T.; Kang, B. R.; Bai, K. H.; Im, Y. H. *Mater. Lett.* **2009**, *63*, 2516.

(15) Guo, Z.; Wei, S.; Shedd, B.; Scaffaro, R.; Pereiraa, T.; Hahn, H. T. *J. Mater. Chem.* **2007**, *17*, 806.

(16) Li, G.; Chen, T.; Yan, B.; Ma, Y.; Zhang, Z.; Yu, T.; Shen, Z.; Chen, H.; Wu, T. *Appl. Phys. Lett.* **2008**, *92*, 173104.

(17) Wang, J.; Tsuzuki, T.; Sun, L.; Wang, X. *J. Am. Ceram. Soc.* **2009**, *92*, 2083.

(18) Chen, T.; Xing, G. Z.; Zhang, Z.; Chen, H. Y.; Wu, T. *Nanotechnology* **2008**, *19*, 435711.

(19) Bera, A.; Basak, D. *Appl. Phys. Lett.* **2008**, *93*, 053102.

(20) Bera, A.; Basak, D. *Appl. Phys. Lett.* **2009**, *94*, 163119.

(21) Bera, A.; Basak, D. *ACS. Appl. Mater. Interfaces* **2009**, *1*, 2066.

(22) Li, J.; Zhao, D.; Meng, X.; Zhang, Z.; Zhang, J.; Shen, D.; Lu, Y.; Fan, X. *J. Phys. Chem. B* **2006**, *110*, 14685.

(23) Zhu, Y. F.; Fan, D. H.; Shen, W. Z. *J. Phys. Chem. C* **2007**, *111*, 10402.

(24) Lu, M. Y.; Song, J.; Lu, M. P.; Lee, C. Y.; Chen, L. J.; Wang, Z. L. *ACS Nano* **2009**, *3*, 357.

(25) Wang, Z.; Liu, X.; Gong, J.; Huang, H.; Gu, S.; Yang, S. *Crys. Growth. Des.* **2009**, *8*, 3911−11.

(26) Greene, L. E.; Law, M.; Goldberger, J.; Kim, F.; Johnson, J. C.; Zhang, Y.; Saykally, R. J.; Yang, P. *Angew. Chem., Int. Ed.* **2003**, *42*, 3031.

(27) Bera, A.; Basak, D. *Chem. Phys. Lett.* **2009**, *476*, 262.

(28) Li, H. Q.; Gao, T.; Wang, Y. G.; Wang, T. H. *Appl. Phys. Lett.* **2005**, *86*, 123117.

(29) Feng, P.; Wan, Q.; Wang, T. H. *Appl. Phys. Lett.* **2005**, *87*, 213111.

AM900686C